

Scaling strong-field interactions towards the classical limit

P. COLOSIMO¹, G. DOUMY¹, C. I. BLAGA¹, J. WHEELER¹, C. HAURI², F. CATOIRE¹, J. TATE¹, R. CHIRLA¹, A. M. MARCH¹, G. G. PAULUS³, H. G. MULLER⁴, P. AGOSTINI¹ AND L. F. DIMAURO^{1*}

¹Department of Physics, The Ohio State University, Columbus, Ohio 43210, USA

²Laboratoire d'Optique Appliquée, ENSTA-CNRS-Ecole Polytechnique, F-91761 Palaiseau, France

³Department of Physics, Texas A&M University, College Station, Texas 77843, USA

⁴FOM AMOLF 407 Kruislaan, 1098 SJ Amsterdam, The Netherlands

*e-mail: dimauro@mps.ohio-state.edu

Published online: 23 March 2008; doi:10.1038/nphys914

In 1964 Keldysh¹ helped lay the foundations of strong-field physics by introducing a theoretical framework that characterized atomic ionization as a process that evolves with the intensity and wavelength of the fundamental field. Within this context, experiments² have examined the intensity-dependent ionization but, except for a few cases, technological limitations have confined the majority to wavelengths below 1 μm . The development of intense, ultrafast laser sources in the mid-infrared (1 $\mu\text{m} < \lambda < 5 \mu\text{m}$) region enables exploration of the wavelength scaling of the Keldysh picture while enabling new opportunities in strong-field physics, control of electronic motion and attosecond science. Here we report a systematic experimental investigation of the wavelength scaling in this region by concurrently analysing the production of energetic electrons and photons emitted by argon atoms interacting with few-cycle, mid-infrared fields. The results support the implicit predictions contained in Keldysh's work, and pave the way to the realization of brighter and shorter attosecond pulsed light sources using longer-wavelength driving fields.

Keldysh¹ described the two main effects an intense low-frequency laser field has on an atom as (1) a bending of the Coulomb potential by the field, forming a sufficiently narrow barrier for the electron to tunnel into the continuum, and (2) an oscillating motion of the free electron induced by the field of strength E and frequency ω . The cycle-averaged kinetic energy of the oscillating electron (ponderomotive energy) is given in atomic units as $U_p = E^2/4\omega^2$. The limit of validity of the Keldysh approach is defined by the condition that the adiabaticity parameter $\gamma = \sqrt{I_p/2U_p} \ll 1$, where I_p is the atom's ionization potential. The Simpleman model³ was the first to exploit a classical analysis in this limit for predicting the electron energy distribution (above-threshold ionization (ATI)) and the relationship between phase and U_p for determining the electron's energy ($2U_p$ maximum). Thus, the concept of sub-cycle ionization in a time-varying field became central for connecting tunnelling (electron release) with a specific phase of the field, whereas, in contrast, phase is undefined in the multiphoton limit ($\gamma \gg 1$). Consequently, tunnelling related to the Simpleman model yields a characteristic electron energy spectrum, which can be measured experimentally. Later, the rescattering model^{4,5} provided the crucial extension to convey the essential physical link between high-harmonic generation and ATI. Again, U_p is central for predicting the maximum harmonic ($I_p + 3.2U_p$)

and electron ($10U_p$) energies. Control of U_p , achieved through intensity or wavelength, is then pivotal for manipulating the energy of the outgoing electron, as well as the physics of the rescattering. Intensity is an obvious experimental control parameter but the combined effect of the exponential growth in the ionization rate and saturation (unity ionization probability) severely limits measurements to a small intensity range. In principle, wavelength is a more effective control knob because $U_p \propto \lambda^2$ and not limited by saturation because the tunnelling rate is independent of λ (ref. 1).

From a theoretical point of view, it is important to explore the influence of wavelength on the character of the ionization process. In principle this is determined by the Keldysh adiabaticity parameter, γ , which depends on the field parameters via U_p , but from a physical perspective there is a significant difference in varying the field strength or the wavelength. Recently, Reiss⁶ has discussed the basis of the tunnelling–multiphoton dichotomy and exposed many shortcomings of the Keldysh approach. For instance, at visible wavelengths the hydrogen ground state is above the saddle point of the potential barrier for $\gamma \approx 1$ and thus the concept of tunnelling is meaningless just when it should become instrumental. In addition, small values of γ imply a complete breakdown of the dipole-length gauge approximation on which the Keldysh picture is built. Reiss⁶ considers the more common situation where $\gamma \ll 1$ is reached by increasing the field strength and not decreasing frequency: by contrast, the potential barrier width and thus the corresponding tunnelling rate are directly altered by a change of intensity but not by a change of wavelength alone. Consequently, the reason why the ionization character would depend on the laser wavelength is not at all intuitive. In fact, Keldysh stated that the cycle-average ionization rate is independent of wavelength at least up to a quasi-static limit defined as $E/\sqrt{2I_p}$ or for the intensity used in the current work, for wavelengths longer than 1.03 μm . The majority of the wavelengths reported in this investigation satisfy the Keldysh criterion for quasi-static ionization.

One aim of this letter is to question the validity of the Keldysh parameter as an appropriate metric of tunnel ionization and the correspondence to the progressive emergence of the Simpleman classical behaviour in the photoelectron energy distribution. Experiments provide a practical path for critical evaluation of this scenario, because realistic theoretical approaches on the basis of efficient numerical methods⁷ become intractable at long wavelengths owing to the large electron momenta.

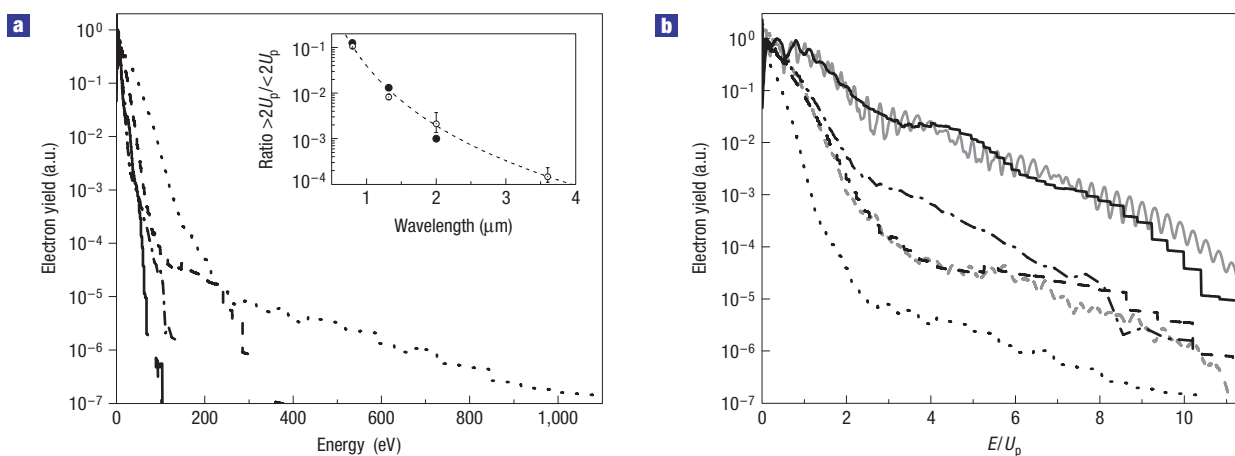


Figure 1 Comparison of photoelectron distributions of argon for different excitations at constant intensity. Excitation is at 0.8 μm (solid line), 1.3 μm (dot–dashed line), 2 μm (dashed line) and 3.6 μm (dotted line) and intensity is 0.08 PW cm^{-2} . **a,b**, The plots are shown in absolute (**a**) and scaled (**b**) energy (normalized against the wavelength-dependent ponderomotive energy). For this intensity U_p is approximately 5 eV, 13 eV, 30 eV and 100 eV for wavelengths of 0.8 μm , 1.3 μm , 2 μm and 3.6 μm , respectively. Also shown in **b** are the TDSE calculations (grey lines) at 0.8 μm (solid line) and 2 μm (dashed line), simulating the experimental conditions (see the Methods section). The agreement between experiment and theory is very good and reproduces the loss of resonant structure at the longer wavelength. The inset in **a** is a plot of the electron yield ratio ($>2U_p / <2U_p$) determined by the experiment (open circle, with error bars) and the TDSE calculations (closed circle) as a function of wavelength. The dashed line illustrates a $\lambda^{-4.4}$ dependence. The 1.3 μm distribution calculated using TDSE is omitted for clarity of presentation but yields similar agreement with the experiment. The resulting 1.3 μm ratio derived from the calculation is plotted in the inset. The error bars reflect the uncertainty in the intensity used in the evaluation of U_p .

Besides the fundamental implications of the current study, the prospect for generating high-quality attosecond bursts also provides a strong motivation. A high-harmonic distribution is characterized by a nearly constant-amplitude frequency comb of odd-order radiation terminating at the cutoff energy given by $I_p + 3.2U_p$ (ref. 8). Obviously, tuning the driver wavelength, λ , longer at fixed intensity produces a denser frequency comb ($\propto \lambda$) with a higher cutoff energy ($\propto \lambda^2$), ingredients needed for synthesis of attosecond pulses. Moreover, the longer-wavelength field is also beneficial for reducing the inherent limitation of the group delay dispersion (attochirp) imposed by the relationship between the electron's initial release time and its instantaneous return energy⁹. Both classical⁹ and quantum⁷ analysis predict that the attochirp scales as λ^{-1} , implying that longer-wavelength fundamental fields produce intrinsically shorter bursts.

Some early experiments using CO_2 lasers ($\lambda \simeq 10 \mu\text{m}$) studied atomic ionization¹⁰ and harmonic generation¹¹. However the CO_2 laser technology was problematic, limited to long pulses and low repetition rate, and thus experiments did not progress significantly. Consequently, essentially all investigations over the past three decades have been carried out using the fundamental or harmonic wavelengths available from titanium sapphire (0.8 μm) or neodymium-based ($\sim 1 \mu\text{m}$) laser systems. Recently, different optical techniques have emerged that enable exploration in the mid-infrared region with sufficient intensity and duty cycle. One attempt in this direction¹² used a wavelength of 1.5 μm for showing that the maximum harmonic energy followed the $3.2U_p + I_p$ cutoff law.

This paper presents the response of argon atoms ionized at a fixed intensity by ultrashort pulses at 0.8, 1.3, 2 and 3.6 μm (see the Methods section). Argon was chosen because both ionization^{13–18} and harmonic generation¹⁹ are well documented at 0.8 μm , thus providing a benchmark for the longer-wavelength results. Furthermore, the variation in the Keldysh parameter ($\gamma \sim 1.3\text{--}0.3$) should be sufficient to observe the evolution from

the multiphoton behaviour at 0.8 μm towards the classical limit at the longest wavelength.

An initial glimpse of the atomic response changing with increasing wavelength is revealed in the measured photoelectron energy distributions shown in Fig. 1. The spectra are recorded at a constant intensity of 0.08 PW cm^{-2} . The maximum electron energy has values of 50 eV, 130 eV, 300 eV and 1 keV at 0.8 μm , 1.3 μm , 2 μm and 3.6 μm , respectively, scaling approximately as λ^2 whereas the maximum number of absorbed photons changes from ~ 40 at 0.8 μm to $\sim 3,000$ at 3.6 μm with only a 4.5 change in the fundamental wavelength ratio.

A more perceptive view of this evolution is illustrated in the scaled energy plot shown in Fig. 1b. A comparison of the distributions reveals some meaningful differences: the 2 μm and 3.6 μm spectra are similar but different from the 0.8 μm case whereas the 1.3 μm result shows a transitional behaviour. These global features provide clear evidence of an evolution: the 0.8 μm distribution shows electron peaks separated by the photon energy (ATI), Rydberg structure near zero energy, a broad resonant enhancement near $4.5U_p$ (refs 13,17,18) and a slowly modulated distribution decaying to $10U_p$ energy. The 2 μm and 3.6 μm distributions have a distinctly different structure: no ATI peaks and a rapid decay from zero to near $2U_p$ energy (Simpleman limit), followed by a plateau extending to $10U_p$ (rescattering limit). The broad resonant enhancement near $4.5U_p$ so well characterized at 0.8 μm (refs 13,17,18) is either completely absent or broadened over a larger energy range. Some additional insight into the changing ionization dynamics is provided by the 1.3 μm distribution, which shows both multiphoton (ATI and broad resonance, although diminishing) and tunnelling (developing classical distribution) character. It therefore appears that the photoelectron evolves closer to the Simpleman behaviour, which is consistent with ionization increasingly approaching the tunnelling regime. The Keldysh parameter with values $\gamma(0.8 \mu\text{m}) = 1.3$, $\gamma(1.3 \mu\text{m}) = 0.8$, $\gamma(2 \mu\text{m}) = 0.5$ and $\gamma(3.6 \mu\text{m}) = 0.3$ at

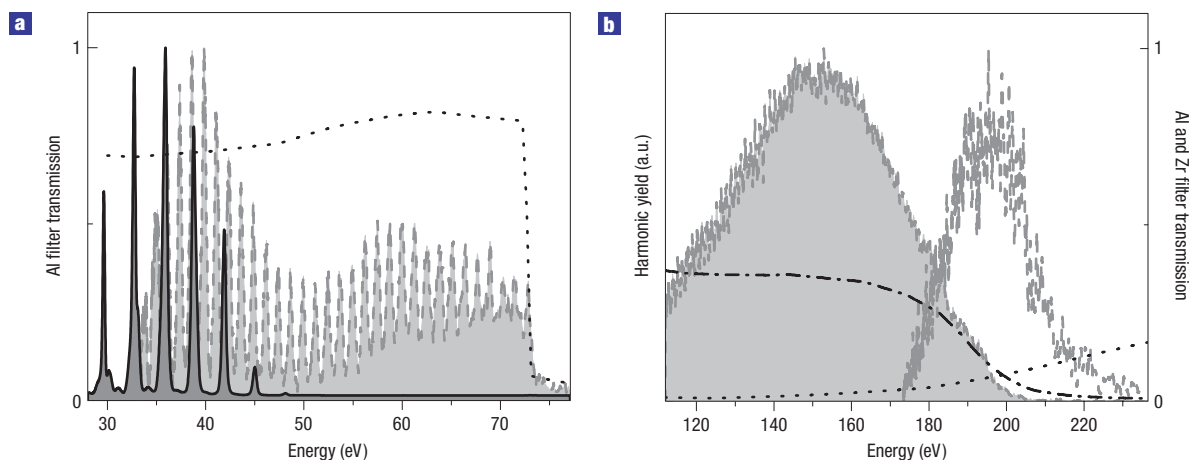


Figure 2 High-harmonic comb produced in argon. The intensity is 0.18 PW cm^{-2} with $0.8 \mu\text{m}$ (solid line) and $2 \mu\text{m}$ (dashed line) pulses. The comb is a continuous series of odd-order harmonics of the fundamental frequency that terminates at an energy defined by the cutoff law. The harmonic spectra at $2 \mu\text{m}$ are recorded in three independent measurements, which have been separately normalized. The harmonics are observed through metal filters, specifically **a**, aluminium, and **b**, zirconium for the low-energy portion and aluminium for high energy. The filter's absolute theoretical transmission curves are plotted for 150-nm-thick aluminium (dotted line) and for 300-nm-thick zirconium (dot-dashed line). The distributions are not corrected for the instrumental response, and reflect notably the efficiency of the blazed gratings.

0.08 PW cm^{-2} provides one rationale for this evolution. However, as stressed above, because the potential barrier width remains constant, this evolution can be attributed only to the fundamental frequency becoming slow compared to the tunnelling frequency, as postulated by Keldysh.

It should be noted that, as the wavelength is increased, the majority of photoelectrons become progressively confined below $2U_p$. This is quantified in the Fig. 1a inset, which shows that the wavelength dependence of the ratio of electrons with energy $> 2U_p$ (rescattered) to those with energy $< 2U_p$ (direct) decreases as $\sim \lambda^{-4}$. One physical interpretation of this scaling is that electrons with energy $> 2U_p$ must have rescattered, and this cross-section declines rapidly with energy and impact parameter. The number of returning electrons with a given kinetic energy decreases by λ^{-2} and the wavepacket's transverse spread scales in area also as λ^{-2} . Consequently, the total decrease in the fraction of rescattered electrons scales as λ^{-4} .

From the perspective of advancing attosecond generation towards shorter durations and wavelengths, evaluating the efficacy for producing high-harmonic combs using long-wavelength fundamental fields is pivotal. Figure 2a shows the argon harmonic distribution in the extreme-ultraviolet region driven by $0.8 \mu\text{m}$ and $2 \mu\text{m}$ fundamental fields, viewed through an Al filter. Currently, harmonic generation is not possible with our $3.6 \mu\text{m}$ source. The focusing optics are chosen to produce the same Rayleigh range at the two different wavelengths and the same intensity ($\approx 0.18 \text{ PW cm}^{-2}$). The $0.8 \mu\text{m}$ distribution shows a 50 eV cutoff (that is, order 31), consistent with previous measurements²⁰, time-dependent numerical results⁷ and the cutoff law⁸. Excitation with $2 \mu\text{m}$ pulses produces a denser (consequence of the smaller photon energy) harmonic comb extending to the Al L edge at $\sim 70 \text{ eV}$ energy. Using a Zr filter instead, the $2 \mu\text{m}$ argon harmonic comb is observed to extend over the entire Zr filter transmission window (60–200 eV) (Fig. 2b). The fast structure is the $2\hbar\omega$ (1.2 eV) spacing whereas the overall shape is a convoluted instrumental response. Obviously, no harmonics are generated in this region using $0.8 \mu\text{m}$ excitation. Measurements using the second Al transmission window establish that the $2 \mu\text{m}$ harmonic cutoff is $\sim 220 \text{ eV}$, which

is consistent with previous calculations⁷ and extends the argon cutoff beyond previous work at $1.5 \mu\text{m}$ (ref. 12).

The above distributions highlight the effectiveness for the λ^2 -scaling to produce higher-energy harmonic photons, but the dependence of the yield is a more difficult quantity to predict theoretically. Numerical solutions of the time-dependent Schrödinger equations (TDSEs) show that the 'single-atom' power-spectrum yield scales as $\lambda^{-5.5 \pm 0.5}$. However, an experiment is a measure of both the atomic response and the macroscopic effects, for example phase matching and propagation. Numerical simulations²⁰ can incorporate both, but comparison with experiment is mostly qualitative. In this regard an experiment is the most reliable metric, although comparison is not always straightforward. We measure the argon harmonic yield at $0.8 \mu\text{m}$ and $2 \mu\text{m}$, while keeping other conditions fixed, for example intensity, argon density, focusing and collection system. Confining the comparison to a spectral bandwidth (35–50 eV) common to both fundamental wavelengths, the $2 \mu\text{m}$ harmonics are observed to be 1,000 times weaker than with $0.8 \mu\text{m}$ and six times less than that predicted by the TDSE calculations⁷. However, independent optimization of only the argon density for maximum harmonic yield at both fundamental wavelengths results in a $2 \mu\text{m}$ yield that is only 85 times weaker. This preliminary, not fully optimized result strongly suggests that the brightness of a $2 \mu\text{m}$ harmonic source can be comparable to a $0.8 \mu\text{m}$ driver in the extreme-ultraviolet region ($\leq 50 \text{ eV}$) and superior at higher energies ($50 \leq \hbar\omega \leq 200 \text{ eV}$). Consistent with our findings, a recent theoretical study²¹ shows that favourable phase matching conditions can be realized at mid-infrared wavelengths.

As the Keldysh parameter $\gamma \ll 1$ and $U_p/\hbar\omega \gg 1$, the demonstration that the photoelectron behaviour tends to the Simpleman classical limit whereas ionization evolves towards pure tunnelling supports the Keldysh view. The scaling of the strong-field physics has important implications for tomographic imaging²² of a broad class of molecular systems, both static and dynamic. Equally important, our findings extended tests of strong-field physics into a domain that had remained hitherto impractical for both experiments and theory. From an application viewpoint, our

study shows that useful amounts of extreme-ultraviolet light can still be obtained from longer-wavelength drivers, despite the drop in efficiency. These observations, coupled with the prediction of a λ^{-1} reduction in the attochirp, define the use of longer-wavelength fundamental fields as a logical road-map towards brighter and shorter attosecond bursts.

METHODS

LIGHT SOURCES

Three separate laser sources generate the wavelengths used in these experiments. The 0.8 μm source is a commercial 3-kHz-repetition-rate titanium sapphire amplifier system (Femtolasers GmbH, model FemtoPower) that produces 0.8 mJ, 30 fs (11 cycles) pulses.

The 1.3 μm and 2 μm source is a modified commercial (Light Conversion, model HE-TOPAS) travelling-wave optical parametric amplifier. It is pumped by 4 mJ, 50 fs pulses originating from a 1 kHz titanium sapphire amplifier system operating at 0.81 μm . First, superfluorescence is generated in a β -barium borate crystal pumped by a small fraction of the titanium sapphire light. In subsequent passes, the same crystal acts as a preamplifier of the wavelength-selected signal beam (for these experiments 1.3 μm). Finally, a 2-mm-long β -barium borate crystal acts as a power amplifier, and is synchronously seeded by the amplified signal and the remaining pump beam in a non-collinear geometry that enables spatial separation of the pump, signal and idler beams, yielding ~ 1 mJ of 1.3 μm and 550 μJ of 2 μm light. A pulse duration of 50 fs (12 cycles at 1.3 μm and seven to eight cycles at 2 μm) was measured using interferometric autocorrelation. The 2 μm focal waist was characterized with a thermal camera, enabling an independent estimate of the intensity.

The 3.6 μm source is a single-pass difference frequency generator. A 0.816 μm beam from a 2.5 mJ, 100 fs, 1 kHz titanium sapphire amplifier system is weakly focused in a potassium titanyl arsenate crystal (dimensions: 5 mm long, 10×10 mm) and mixed with pulses from a 16 ps, 0.8 mJ, 1 kHz Nd:YLF regenerative amplifier system, operating at 1.053 μm . The mode-locked oscillators of the two laser systems are synchronized to a stable rf source with jitter ≤ 1 ps. The two amplified beams overlap in the mixing crystal at a small angle, enabling spatial separation of the different wavelengths. Pulses are generated at 3.6 μm with an energy of 0.18 mJ. A 150 fs pulse (12 cycles) duration is measured using interferometric autocorrelation. The low 3.6 μm pulse energy prohibits the generation of high harmonics from argon.

TDSE CALCULATIONS

The code²³ used for solving the TDSE has been thoroughly described and validated in previous studies^{7,18}. The model argon atom, initially in the ground state, is treated in the single-active-electron approximation with spin-orbit coupling ignored. The code outputs the angle-resolved photoelectron energy distribution and the time-dependent acceleration of the dipole, from which the harmonic spectra are obtained by Fourier transformation. The wavelengths investigated are between 0.8 and 2 μm . For longer wavelengths, the calculation becomes intractable owing to the computational demands on the grid size of the integration box and the time steps resulting from the high velocity of the electron wavepacket. For comparison with the experiment in Fig. 1b, the calculated photoelectron distributions are spatially and temporally averaged over the focal volume.

PHOTOELECTRON SPECTROMETER

The photoelectron energy distributions are recorded using a time-of-flight arrangement. The laser pulses are focused by a $f/5$ lens and the resulting electrons detected at the end of a field-free, magnetically shielded flight tube (23 cm) by a 40-mm-diameter microchannel-plate chevron assembly. The photoelectrons are collected in a 5° solid angle. The microchannel-plate signal is amplified and recorded by a time-to-digital converter with a 1 ns resolution, yielding an energy resolution of 5%. Depending on the intensity, the argon density is adjusted to produce ~ 1 electron per shot. The measurement of the

less abundant plateau photoelectron from argon requires a vacuum-chamber base pressure of 10^{-10} torr to minimize background contributions.

HARMONIC SOURCE AND EXTREME-ULTRAVIOLET SPECTROMETER

The high harmonics are generated by focusing the laser pulses into a static gas cell, operating with a continuous gas flow. The cell is a thin (1.5 mm) rectangular-cross-section metal nozzle wrapped in Teflon, backed with a pressure of up to 250 torr. After alignment, the laser drills a hole through the Teflon, ensuring minimal gas load on the pumps and limiting reabsorption (the pressure in the generation chamber is kept to 10^{-3} – 10^{-4} torr).

The soft-X-ray spectrometer is differentially pumped with respect to the harmonic source chamber with the gas cell placed at the spectrometer's entrance plane. The 0.5 m Hettrick design (Hettrick Scientific) operates at a 2° grazing angle and has three different dispersion gratings. A Kirkpatrick–Baez mirror geometry collects and focuses the soft-X-ray radiation on the exit plane. The dispersed spectrum is detected on a back-illuminated soft-X-ray CCD (charge-coupled device) camera (Andor). Before the spectrometer optics, different metal filters (Al or Zr, depending on the wavelength range studied) are used to suppress the fundamental and low-order harmonic light.

Received 17 July 2007; accepted 13 February 2008; published 23 March 2008.

References

- Keldysh, L. V. Ionization in the field of a strong electromagnetic wave. *Sov. Phys. JETP* **20**, 1945–1950 (1964).
- Augst, S., Strickland, D., Meyerhofer, D. D., Chin, S. L. & Eberly, J. H. Tunneling ionization of noble gases in a high-intensity laser field. *Phys. Rev. Lett.* **63**, 2212–2215 (1989).
- van Linden van den Heuvell, H. & Muller, H. in *Multiphoton Processes* (eds Smith, S. J. & Knight, P. L.) 25–34 (Cambridge Univ. Press, Cambridge, 1988).
- Schafer, K. J., Yang, B., DiMauro, L. F. & Kulander, K. C. Above threshold ionization beyond the high harmonic cutoff. *Phys. Rev. Lett.* **70**, 1599–1602 (1993).
- Corkum, P. B. Plasma perspective on strong field multiphoton ionization. *Phys. Rev. Lett.* **71**, 1994–1997 (1993).
- Reiss, H. Inherent contradictions in the tunneling–multiphoton dichotomy. *Phys. Rev. A* **75**, 031404 (2007).
- Tate, J. *et al.* Scaling of wave-packet dynamics in an intense midinfrared field. *Phys. Rev. Lett.* **98**, 013901 (2007).
- Krause, J. L., Schafer, K. J. & Kulander, K. C. High-order harmonic generation from atoms and ions in the high intensity regime. *Phys. Rev. Lett.* **68**, 3535–3538 (1992).
- Mairesse, Y. *et al.* Attosecond synchronization of high-harmonic soft X-rays. *Science* **302**, 1540–1543 (2003).
- Corkum, P. B., Burnett, N. H. & Brunel, F. Above-threshold ionization in the long-wavelength limit. *Phys. Rev. Lett.* **62**, 1259–1262 (1989).
- Carman, R. L., Forslund, D. W. & Kindel, J. M. Visible harmonic emission as a way of measuring profile steepening. *Phys. Rev. Lett.* **46**, 29–32 (1981).
- Shan, B. & Chang, Z. Dramatic extension of the high-order harmonic cutoff by using a long-wavelength driving field. *Phys. Rev. A* **65**, 011804 (2001).
- Paulus, G. G., Grasbon, F., Walther, H., Kopold, R. & Becker, W. Channel-closing-induced resonances in the above-threshold ionization plateau. *Phys. Rev. A* **64**, 021401 (2001).
- Muller, H. G. & Kooiman, F. C. Bunching and focusing of tunneling wave packets in enhancement of high-order above-threshold ionization. *Phys. Rev. Lett.* **81**, 1207–1210 (1998).
- Wassaf, J., Vénier, V., Taieb, R. & Maquet, A. Strong field atomic ionization: Origin of high-energy structures in photoelectron spectra. *Phys. Rev. Lett.* **90**, 013003 (2003).
- Potvliege, R. M. & Vučić, S. High-order above-threshold ionization of argon: Plateau resonances and the Floquet quasienergy spectrum. *Phys. Rev. A* **74**, 023412 (2006).
- Hertlein, M. P., Bucksbaum, P. H. & Muller, H. G. Evidence for resonant effects in high-order ATI spectra. *J. Phys. B* **30**, L197–L205 (1997).
- Nandor, M. J., Walker, M. A., Van Woerkom, L. D. & Muller, H. G. Detailed comparison of above-threshold-ionization spectra from accurate numerical integrations and high-resolution measurements. *Phys. Rev. A* **60**, R1771–R1774 (1999).
- Hergott, J. F. *et al.* Extreme-ultraviolet high-order harmonic pulses in the microjoule range. *Phys. Rev. A* **66**, 021801 (2002).
- Lopez-Martens, R. *et al.* Amplitude and phase control of attosecond light pulses. *Phys. Rev. Lett.* **94**, 033001 (2005).
- Yakovlev, V. S., Ivanov, M. & Krausz, F. Enhanced phase-matching for generation of soft X-ray harmonics and attosecond pulses in atomic gases. *Opt. Express* **15**, 15351–15364 (2007).
- Itatani, J. *et al.* Tomographic imaging of molecular orbitals. *Nature* **432**, 867–871 (2004).
- Muller, H. G. Numerical simulation of high-order above-threshold-ionization enhancement in argon. *Phys. Rev. A* **60**, 1341–1350 (1999).

Acknowledgements

This work was carried out with support from USDOE/BES under contracts DE-FG02-04ER15614 and DE-FG02-06ER15833. L.F.D. acknowledges support from the Hagenlocker chair. We are grateful to L. Young (Argonne National Laboratory) for the loan of the Hettrick spectrometer. Correspondence and requests for materials should be addressed to L.F.D.

Reprints and permission information is available online at <http://npg.nature.com/reprintsandpermissions/>